THE JOURNAL OF PHYSICAL CHEMISTRY B

Article

pubs.acs.org/JPCB

The Protein Environment of the Bacteriopheophytin Anion Modulates Charge Separation and Charge Recombination in Bacterial Reaction Centers

Jie Pan,*[,†,#] Rafael G. Saer,[§] Su Lin,[†,‡] Zhi Guo,[†] J. Thomas Beatty,[§] and Neal W. Woodbury*[,†,‡]

[†]The Biodesign Institute at Arizona State University, Arizona State University, Tempe, Arizona 85287-5201, United States

[‡]Department of Chemistry and Biochemistry, Arizona State University, Tempe, Arizona 85287-1604, United States

[§]Department of Microbiology and Immunology, The University of British Columbia, 2350 Health Sciences Mall, Vancouver, British Columbia, Canada V6T 1Z3

Supporting Information

ABSTRACT: The kinetics and pathway of electron transfer has been explored in a series of reaction center mutants from *Rhodobacter sphaeroides*, in which the leucine residue at M214 near the bacteriopheophytin cofactor in the A-branch has been replaced with methionine, cysteine, alanine, and glycine. These amino acids have substantially different volumes, both from each other and, except for methionine, from the native leucine. Though the mutation site of M214 is close to the bacteriopheophytin cofactor, which is involved in the electron transfer, none of the mutations alter the cofactor composition of the reaction center and the primary charge separation reaction is essentially undisturbed. However, the kinetics of electron transfer from H_A^- → Q_A becomes both slower and substantially heterogeneous in three of the four mutants. The decreased H_A^- → Q_A electron transfer rate allows charge recombination between P^+ and H_A^- to compete with the forward reaction, resulting in a drop in the overall yield of charge separation. Both the yield change and the variation in kinetics correlate well with the volume of the mutant amino acid side chains. Analysis of the kinetics suggests that the introduction of a smaller side chain at M214 results in greater protein structural heterogeneity and dynamics on multiple time scales, resulting in perturbation of the electronic environment and its evolution in the vicinity of the early charge-separated radical pair, $P^+H_A^-$, and the subsequent acceptor Q_A, affecting both the extent and time scale of dielectric relaxation. It appears that the reaction center has been optimized not only in terms of its static structure−function relationships, but also finely tuned to favor particular reaction pathways on particular time scales by adjusting protein dynamics.

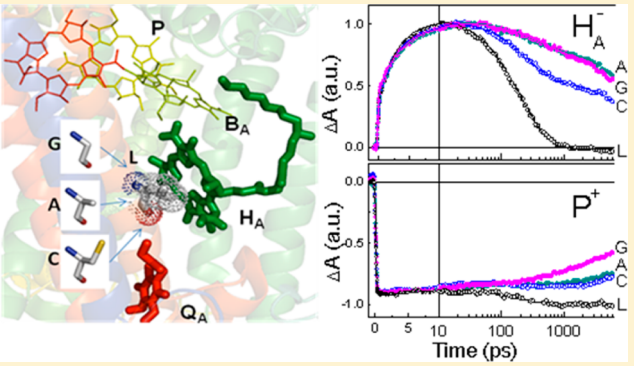

INTRODUCTION

The multistep design of photosynthetic electron transfer chains is common across species and is a key contributor to the near unity quantum efficiency of the light-energy conversion reaction in reaction centers of photosynthetic systems. Inherent in the structure−function relationship in these systems is the need for the cofactor and surrounding protein environment to be optimized for each of the electron transfer reactions, which occur sequentially on very different time scales and with very different driving forces.[1−3] Electron transfer, like all chemical reactions, depends not only on the structure of the molecular system involved, but also on molecular dynamics. Reactions that occur on very different time scales likely depend on different molecular sources of motion, particularly within structurally constrained environments like a protein.[4−7] Thus at any particular point in the photosynthetic electron transfer chain, Nature is presented with the challenge of optimizing the dynamics of a single structure to support multiple reactions on multiple time scales.[8,9]

The photosynthetic reaction center of purple nonsulfur bacteria is probably the best studied example of this kind of multistep light-induced electron transfer system. It is also, perhaps, uniquely suited for the detailed study of the role of protein dynamics in electron transfer chains because of its simplicity, its robustness, the distinct spectral characteristics of each cofactor, and the multiple electron transfer reactions that occur across time scales from picoseconds (ps) to seconds (for reviews, see refs 1−3,10,11). Figure 1a shows the cofactor arrangement in the reaction center of *Rhodobacter (Rb.) sphaeroides*.[12,13] The electron transfer reaction is initiated when light is absorbed by a bacteriochlorophyll (BChl) dimer, P. The excited P transfers an electron to a bacteriopheophytin (BPhe), H_A, via a monomer BChl (B_A), followed by an electron transfer to the first of two quinones,

Received: January 4, 2013
Revised: May 10, 2013

   dx.doi.org/10.1021/jp400132k | *J. Phys. Chem. B* XXXX, XXX, XXX−XXX

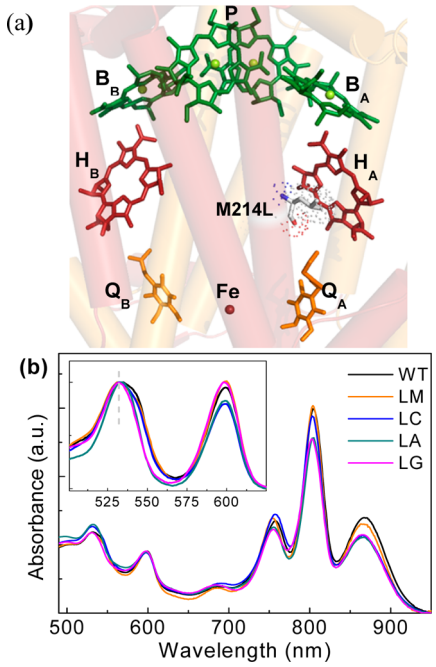

Figure 1. (a) Structure of the wild type *Rb. sphaeroides* reaction center cofactors (PDB code: 2J8C). The BChl dimer, P, and the two monomer-BChls, B, are shown in green, and the BPhes are shown in red. For clarity, the phytyl tails of all bacteriochlorin molecules are truncated. The first quinone molecule, Q_A, is shown in orange, and the second one, Q_B, in yellow. The nonheme iron is represented by an orange ball. The position of leucine (L) M214 in the structure of wild type reaction centers is also shown. (b) Room temperature absorption spectra of reaction centers from the wild type and four M214 mutants. Inset: comparison of the Q_X transition bands of H_A, H_B, and B/P at 540, 530, and 600 nm, respectively, with the contribution of carotenoid absorption in this wavelength region subtracted. The vertical marker indicates wavelength of 530 nm where all spectra are normalized.

Q_A, and finally to the second quinone, Q_B. The back reactions at each step are 2−4 orders of magnitude slower than the forward reactions, resulting in a quantum yield near unity.

In this trans-membrane electron transfer chain, the BPhe at the H_A site is involved in at least three reactions. It receives an electron from B_A^- on the picosecond time scale forming $P^+H_A^-$,[14,15] it transfers an electron to Q_A on the hundred picosecond time scale forming $P^+Q_A^-$, and it is able to undergo charge recombination from H_A^- to P^+ (a reaction Nature tries to avoid) with a time constant on the nanosecond (ns) time scale. In wild type reaction centers, the 200-ps forward reaction to the quinone[16,17] out-competes the 10−20 ns $P^+H_A^-$ recombination reaction almost completely. The rate of $P^+H_A^-$ recombination has been determined in the absence of forward electron transfer by removing or reducing Q_A.[18−25] Under these conditions, the relative free energy of $P^+H_A^-$ has been shown to decrease with time due to relaxation of the protein environment over hundreds of picoseconds to nanoseconds, a process revealed by monitoring the multiexponential time dependence of the P* fluorescence after P* and $P^+H_A^-$ achieve a quasi-equilibrium.[7,20,22,26−29]

By varying the relative energetics between the cofactors via mutagenesis, it has been possible to study the relationship between rate and driving force in electron transfer. In particular, the effects of changing the P^+/P oxidation potential and the Q_A/Q_A^- reduction potential have been studied in some detail.[30,31] Less is known about the role of the H_A/H_A^- midpoint potential in modulating electron transfer kinetics. One of the reasons for this is that there are very few mutants in which the redox properties of H_A have been systematically varied, due in part to the difficulty of directly measuring this parameter. One H_A mutant that significantly impacts the $H_A^- \rightarrow Q_A$ electron transfer kinetics is the so-called β mutant (M214LH), in which the BPhe at the H_A binding site is replaced by a BChl molecule (denoted as β).[32] In this mutant, the driving force between $P^+B_A^-$ and $P^+\beta_A^-$ is nearly zero. The overall forward electron transfer rate from P* to β_A slows to 6 ps, and the rate from β_A to Q_A slows to 580 ps. Charge recombination in $P^+\beta_A^-$ occurs with a time constant of about 1 ns, an order of magnitude faster than in the wild type reaction center, resulting in a 40% yield loss during the $\beta_A^- \rightarrow Q_A$ reaction. Further elevation of the energy level of β_A via addition of a hydrogen bond in the mutant M214LH+L104LE resulted in an even larger $\beta_A^- \rightarrow Q_A$ yield loss (70%).[33]

The coupling of protein dynamics and electron and energy transfer has been shown to be an important factor both in controlling reaction pathways and in determining the degree and time scale of dielectric relaxation of the protein upon charge separation.[8,34−39] An obvious but important consideration in understanding the role of protein dynamics in electron transfer is that reactions, which occur with widely different rates, are necessarily coupled to different kinds of protein dynamics. The P* $\rightarrow$ H_A electron transfer reaction occurs on the picosecond time scale where protein movement is limited and generally not associated with changes in the tertiary structure of the protein. The $H_A^- \rightarrow Q_A$ electron transfer reaction, on the other hand, occurs on a time scale of hundreds of picoseconds. Here, the molecular dynamic repertoire becomes more complex,[26,27,29,40] and collective protein motions begin to come into play. These dynamics directly affect the rates of both forward electron transfer from $H_A^- \rightarrow Q_A$ and of unproductive $P^+H_A^-$ recombination. The long-range dynamic modes are much more strongly dependent on tertiary structure than are picosecond dynamics.[40−43]

In the *Rb. sphaeroides* reaction center, M214 is the residue altered in the so-called β mutant described above, in which a metal coordination site is introduced next to the H_A cofactor, so the M214 side chain plays a key role in determining the protein environment affecting the electron transfer reactions involving H_A.[32] In this work, additional mutations of this residue are explored that, unlike the β mutant, do not change the BPhe to BChl in the H_A site. Specifically, four mutants were considered, in which methionine, cysteine, alanine, and glycine replaced the M214 leucine present in the wild type reaction center. These amino acids have substantially different molecular volumes, both from each other and, except for methionine, from the native leucine. Increasing the space available around the H_A site should allow for different types of protein motion or possibly a different distribution of internal waters in the system. In either case, protein dynamics and dielectric relaxation should be perturbed directly in a critical region of the protein structure that controls the rate and yield of both the initial and secondary electron transfer reactions.

MATERIALS AND METHODS

Creation of M214 Mutant Reaction Center Genes. The plasmid pAli2, containing the *puf QBALMX* genes of *Rb. sphaeroides* on a 4.6-kb *Eco*RI fragment, was modified by site-directed mutagenesis using the primer 5′-CTCTACGGGTC-

dx.doi.org/10.1021/jp400132k | J. Phys. Chem. B XXXX, XXX, XXX−XXX

GGCCXXXCTCTTCGCGATGCAC-3′, and its reverse complement, where XXX represents the codon for methionine, cysteine, alanine, or glycine. The desired changes were confirmed by DNA sequencing of both the *pufL* and *pufM* genes.[44] The mutant reaction center genes were subcloned into a derivative of plasmid pRS1, which contains a modified *puhA* (reaction center H subunit) gene encoding a C-terminal 6-histidine tag transcriptionally upstream of the mutant reaction center M gene in the *puf* operon. This plasmid was transferred to *Rb. sphaeroides* strain ΔRCLH via conjugation.[45]

Growth of Bacterial Cultures and Reaction Center Purification. *Rb. sphaeroides* strains containing mutant reaction center genes were grown chemotrophically at 30 °C in 1400 mL of LB medium[46] supplemented with 810 μM $MgSO_4$, 510 μM $CaCl_2$, and 1 mg/L thiamine-HCl, using 2 L Erlenmeyer flasks shaken at 150 rpm. Purification of the reaction centers was carried out according to a modified version of the protocol from Goldsmith and Boxer.[47] Membrane vesicles (chromatophores) were solubilized with lauryl dimethyl amine oxide (LDAO) in a buffer of 10 mM Tris-HCl (pH 8.0) and 100 mM NaCl; imidazole was added to the solubilized protein solution to yield a concentration of 5 mM. The His-tagged reaction center was bound to a Ni^{2+}-NTA column (Qiagen) and was then washed with 10 mM Tris-HCl (pH 8.0), 100 mM NaCl, and 0.1% LDAO to eliminate the absorbance at 875 nm in the flow-through solution. The mixture was then eluted in the same solution containing 300 mM imidazole. Imidazole and NaCl were removed from the reaction center solution by dialysis against 10 mM Tris-HCl (pH 8.0), 0.1% LDAO. For spectroscopic measurements, reaction centers were in a solution of 10 mM Tris-HCl (pH 8.0), 0.1% LDAO, and 10 mM orthophenanthroline to block the Q_A to Q_B electron transfer.

Femtosecond Transient Absorption Spectroscopy. The femtosecond transient absorbance spectrophotometer has been described previously.[48] Briefly, 1 mJ laser pulses at a repetition rate of 1 kHz (100 fs pulse duration at 800 nm), were generated from a regenerative amplifier system (Tsunami and Spitfire, Spectra-Physics). Part of the pulse energy (600 μJ) was used to pump an optical parametric amplifier (OPA-800, Spectra-Physics) to generate 865-nm excitation pulses. Excitation at 865 nm was used for all measurements as this directly generates the lowest excited singlet state of P. Transient absorption changes at various wavelengths were measured by using a spectrophotometer coupled with a CCD camera (DU420, Andor Technology). The polarization of the pump pulses was set to the magic angle (54.7°) with respect to that of the probe pulses. Measurements were performed in two overlapping spectral regions: visible (500−760 nm) and near-IR (680−980 nm), in order to interrogate the Q_X and Q_Y transitions, respectively, of the reaction center bacteriochlorins. Data was collected over a time range from 0.5 ps before to 6 ns after the excitation pulse. Reaction center samples were loaded in a spinning wheel with an optical path length of 1.2 mm at a final optical density of ~0.8 at 800 nm. All measurements were performed at room temperature. Time-resolved spectra were corrected for spectral dispersion, and data analysis was performed using a global fitting program as described previously.[48,49]

RESULTS

Figure 1b compares the ground-state absorbance spectra of the wild type reaction center and four mutants, in which leucine (L) at position M214 is replaced with methionine (M214LM), cysteine (M214LC), alanine (M214LA), or glycine (M214LG). The Q_Y transitions of the H, B, and P cofactors peak near 760, 802, and 865 nm, respectively, for all of the samples. The Q_X transitions of B and P are both near 600 nm, and the Q_X transitions of H are located near 540 nm. For these mutants, there is no indication that the BPhe has been converted to a BChl as in the case of the so-called *β* mutant. In the *β* mutant, the conversion of the BPhe at the H_A binding site to a BChl molecule results in a decrease in amplitude of the BPhe bands near 540 and 760 nm, and amplitude increases of the bands near 600 and 780 nm.[32] None of those spectral changes are apparent in M214LM, M214LC, M214LA, or M214LG. A comparison of the H (BPhe), B (BChl), and P bands in the Q_X region after the subtraction of the background signals from the carotenoid absorption in the 460−560 nm region (inset of Figure 1b) shows that the ratio of the amplitudes of the 540 and 600 nm bands are similar for all reaction centers, although the Q_X band of the BPhe molecules is slightly narrowed on the long wavelength side for the M214LA and M214LG mutant reaction centers, likely due to changes in the protein environment of the H_A BPhe.

Primary Electron Transfer. The initial electron transfer reaction is thought to involve two sequential steps; $P^* \rightarrow P^+B_A^-$ and $P^+B_A^- \rightarrow P^+H_A^-$. As illustrated in the time-dependent wild type reaction center absorbance difference spectra (Figure 2a inset), following laser excitation the reaction

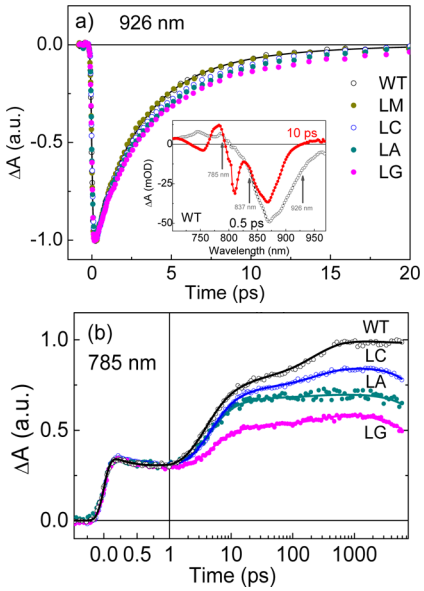

Figure 2. Normalized kinetic traces for reaction center samples from wild type (black open circles), M214LC (blue open circles), M214LA (dark cyan filled circles), M214LG (magenta filled circles), and M214LM (dark yellow filled circles). The excitation wavelength was 865 nm. Panel a: The probe wavelength was 926 nm; the solid line represents a single exponential fit of the wild type sample with a time constant of 3.5 ps. Inset: comparison of transient absorbance difference spectra in the Q_Y spectral region at 0.5 ps (black) and 10 ps (red) after 865-nm excitation of wild type reaction center samples. Arrows at 785, 837, and 926 nm highlight the probe wavelengths of the kinetic traces shown in this figure, panel b, Figure 3d, and this figure, panel a, respectively. Panel b: The probe wavelength was 785 nm; the color code is as in panel a. The kinetics of the M214LM mutant are identical to those of the wild type (data not shown). Note that the time axis is linear until 1 ps and then logarithmic to 6 ns.

dx.doi.org/10.1021/jp400132k | J. Phys. Chem. B XXXX, XXX, XXX−XXX

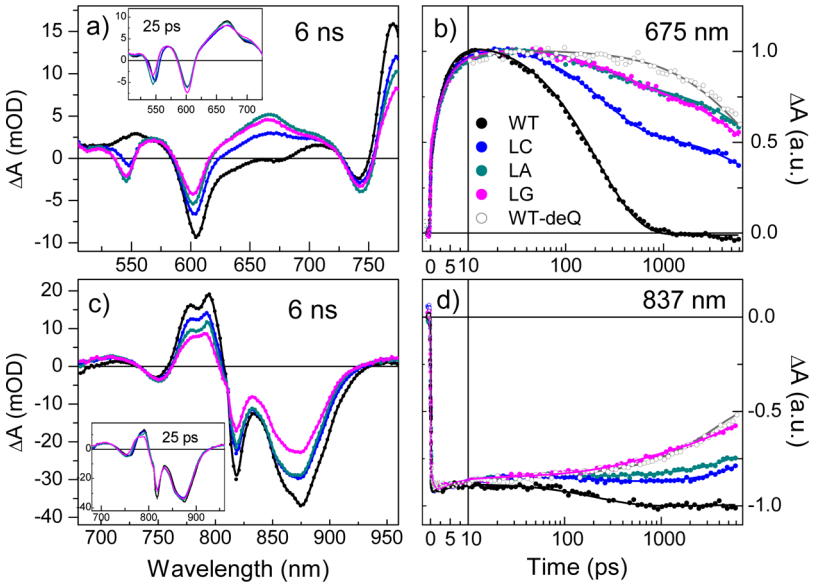

Figure 3. Left panels (a and c): transient absorbance difference spectra of wild type (black), M214LC (blue), M214LA (green), and M214LG (magenta) mutant reaction centers in the Q_X (a) and Q_Y (c) spectral regions recorded at 6 ns time delay following excitation at 865 nm. The time vs wavelength spectral surface for each sample was normalized to the bleaching maximum at 0.5 ps and either 600 nm (Q_X region) or 865 nm (Q_Y region). In this way, all absorbance changes should reflect differences relative to the same amount of initial P* generated. Insets: transient absorbance difference spectra recorded at 25 ps time delay in the Q_X (a, inset) and Q_Y (c, inset) region. Right panels (b and d): normalized kinetic traces recorded for reaction center samples from wild type, and the M214LC, M214LA, and M214LG mutants at probe wavelengths 675 nm (b) and 837 nm (d) upon excitation at 865 nm. Color codes are the same as in left panels. Kinetic traces from wild type reaction centers from which the Q_A quinone was removed (WT-deQ) are shown in gray for comparison. Symbols are experiment data, and the solid lines represent the fitting results generated using global analysis. Note that the time axis is linear until 10 ps and then logarithmic to 6 ns.

center proceeds from P*, which dominates the 0.5-ps spectrum, to the $P^+H_A^-$ charge-separated state at 10 ps. Much of the absorbance decrease present for wavelengths greater than 850 nm at 0.5 ps recovers over the subsequent few picoseconds due to the decay of the stimulated emission from P* as charge separation occurs. By monitoring the signal between 920 and 930 nm, the kinetics of P* stimulated emission decay, and thus the initial electron transfer reaction can be measured with minimal contribution from the P ground-state bleaching band centered near 865 nm. The distinction between stimulated emission (P*) decay and ground-state bleaching recovery is important in the analysis of mutants with charge separation quantum yields of less than unity.

The kinetics of P* decay at 926 nm in the wild type and M214 mutant reaction centers is compared in Figure 2a. The P* stimulated emission decay is very similar in all mutants and the wild type, with most of the decay taking place within a few ps for all samples. The small differences that are observed between the mutants are most pronounced after 5 ps, particularly for the M214LG mutant, though even this kinetic difference is small compared to the kinetic changes observed previously in the β mutant, where the single exponential lifetime of P* was increased by roughly a factor of 2 from ~3 ps in wild type to ~6 ps.[33] The simplest interpretation of this is that replacing M214 with methionine, cysteine, alanine, or glycine gives rise to much smaller energetic changes than does the histidine replacement in the β mutant reaction center.

In the wild type reaction center, the P* → $P^+B_A^-$ reaction has a time constant of about 3 ps, whereas the $P^+B_A^-$ → $P^+H_A^-$ reaction is faster, with a time constant of less than 1 ps.[14,15] The kinetics around 785 nm shows the characteristic absorbance changes in the first picosecond that are due to an electrochromic shift of the B_A ground state absorbance band that accompanies the formation of $P^+H_A^-$ from P* via $P^+B_A^-$.[14,15] Figure 2b compares the kinetics measured at 785 nm from the wild type and the M214L(C/A/G) mutant reaction centers (the M214LM kinetic trace is not shown as it is identical to wild type). During the first picosecond, the traces from all of the mutants are essentially the same as wild type, suggesting that the kinetics of both steps in the P* → $P^+B_A^-$ → $P^+H_A^-$ reaction sequence are very similar in wild type and the M214 mutants studied here.

Secondary Electron Transfer to Q_A and Charge Recombination. Once $P^+H_A^-$ is formed, the H_A anion state (H_A^-) can decay by one of two pathways: forward electron transfer ($P^+H_A^-$ → $P^+Q_A^-$), or charge recombination (return of the electron from H_A^- to P^+, reforming the ground state). The contribution from each pathway can be determined by following the absorbance changes induced by H_A^- and P^+ separately. The kinetics at 675 nm reflects the population change of H_A^-. Its decrease on the hundreds of picosecond to nanosecond time scale is a result of forward electron transfer and $P^+H_A^-$ charge recombination, whereas the decrease of the P band signal at 837 nm is mainly due to the $P^+H_A^-$ recombination. Figure 3 panels a and c compare the transient absorbance difference spectra of the mutants and wild type at 25 ps (inset) and 6 ns after excitation. For the analysis that follows, transient difference spectra of all samples were normalized to their absorbance change spectra at 0.5 ps such that they all have the same P* bleaching at 600 and 865 nm in the Q_X and Q_Y spectral regions, respectively. This allows comparative analysis of the relative yield of each state in the different reaction center samples. At 25 ps after 865 nm excitation (Figure 3a, inset), reaction centers are in the state $P^+H_A^-$, as demonstrated by the spectral features in the Q_X region. Wild type reaction centers and all of the M214 mutants

dx.doi.org/10.1021/jp400132k | J. Phys. Chem. B XXXX, XXX, XXX–XXX

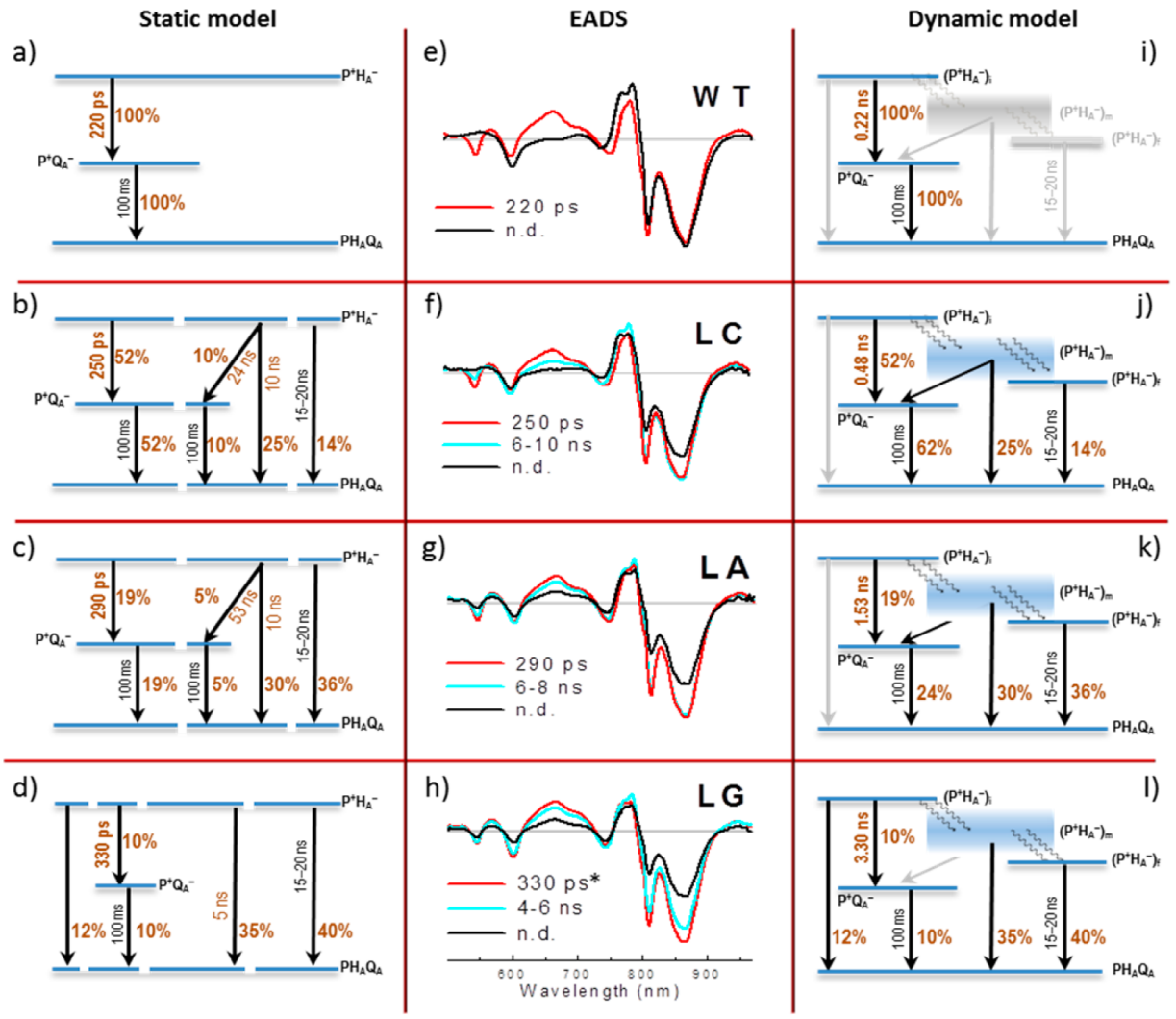

Figure 4. Middle panels: EADS of components associated with H_A^- decay and P^+ charge recombination from reaction centers of (e) wild type; (f) M214LC; (g) M214LA; and (h) M214LG. Fitting lifetimes are shown as the legends (n.d. = non-decaying). (*: The hundreds of picosecond lifetime, red curve, in the Q_Y region is 430 ps). Left panels (a to d): reaction schemes for each sample based on a static heterogeneity model, showing the relevant states, reaction pathways, time constants, and yields that result from the model (see text for details). Right panels (i to l): reaction scheme constructed based on a dynamic heterogeneity model, illustrating the relevant states, relaxation pathways, time constants, and yields resulting from application of this model. In both models, the dominant reaction pathways are indicated by solid black arrows, pathways that are not appreciable used in a particular type of reaction center are shown in gray. The blue region with wavy arrows represents a continuous relaxation from $(P^+H_A^-)_i$ to $(P^+H_A^-)_f$. The details of the calculation of the rates and yields along each reaction path are given in the Supporting Information and the results are listed in Table 3.

contain two negative bands at ~545 and 600 nm, and a broad positive band peaking at ~660 nm. The two negative bands are due to bleaching of H_A and P after charge separation, respectively, and the absorbance increase is due to H_A anion absorption. Correspondingly, the absorbance difference spectrum in the Q_Y region (Figure 3c, inset) shows a characteristic P^+ signal due to bleaching of P near 865 nm. Note that the amplitude of the 600 nm bleaching in the M214LG mutant is about 5−10% larger and the H_A anion-associated signals are somewhat smaller than those of wild type and other mutants. In addition, the 600 nm bleaching at 25 ps is a few percent larger than it is at 0.5 ps with the bleaching maximum being 2 nm blue-shifted (data not shown). One interpretation of these observations is that there is a small population of $P^+B_A^-$at 25 ps. This could be due to either a slower $B_A^- \rightarrow H_A$ electron transfer or an equilibrium between the populations in the $P^+B_A^-$ and $P^+H_A^-$ states in the M214LG mutant, but given the similarity of the 785 nm kinetics in M214LG and the other samples, equilibration seems most likely. As with the initial electron transfer kinetics, the M214LG mutant shows the largest deviation from wild type.

At 6 ns after laser excitation, the difference in transient absorption spectra between the wild type and mutant reaction centers is much greater than at 25 ps (Figure 3 panels a and c). In the wild type reaction center, $P^+Q_A^-$ is formed on a 200-ps time scale, and this state lives for milliseconds.[11] Thus, in the wild type reaction center on the nanosecond time scale, ground-state bleaching of P at both 600 and 865 nm remains unchanged, whereas the H_A ground-state bleaching at 540 nm, as well as the H_A^- band near 660 nm, has disappeared (Figure 3a,c, black curve). The M214LM mutant has the most similar spectral features and decay kinetics for P^+ and H_A^- compared to wild type (Figure S-1, Supporting Information). In contrast, the H_A^- absorbance changes at 540 and 660 nm are still quite

dx.doi.org/10.1021/jp400132k | J. Phys. Chem. B XXXX, XXX, XXX−XXX

pronounced in the other three mutants at 6 ns, implying that these reaction centers remain at least partially in the $P^+H_A^-$ state at this time. Furthermore, the relative amounts of $P^+H_A^-$ and $P^+Q_A^-$ on this time scale vary from mutant to mutant. Of these mutants, the M214LC reaction center has the largest ratio of P^+ signal to H_A^- signal, implying that it has the highest population of $P^+Q_A^-$ at 6 ns. The M214LA and M214LG mutants both have a stronger H_A^- signal relative to P^+, implying that at this time the $P^+H_A^-$ state is still dominant in these two mutants (a quantitative analysis is provided in the Discussion).

The kinetic traces associated with H_A^- (Figure 3b) and P^+ (Figure 3d) are consistent with the spectral results described above. The decay of the anion band at 675 nm in wild type reaction centers is rapid, with a time constant of ~200 ps, due to electron transfer from H_A^- to Q_A (Figure 3b). Since the forward electron transfer rate is ~50 times faster than recombination, a very high yield of $P^+Q_A^-$ is achieved in the wild type reaction center, as indicated by the lack of decay in the ground-state bleaching band of P at 837 nm in our measurement (Figure 3d). In contrast, with the exception of M214LM (Supporting Information, Figure S-1d), the overall 675 nm H_A^- decay is much slower in the M214 mutants than in wild type. In fact, the M214LG and M214LA mutants have H_A^- decay kinetics with components that are nearly as slow as they are in wild type reaction centers in which Q_A has been removed (Figure 3b, gray curve). In addition, the P ground-state bleaching at 837 nm partially recovers during the first few nanoseconds in mutant reaction centers (Figure 3d), indicating that $P^+H_A^-$ recombination effectively competes with the slow forward electron transfer from H_A^- to Q_A. The amplitudes of the recovery of the P ground state signal in M214LC and M214LA reaction centers are similar to each other but less than that in M214LG (Figure 3d), even though the decay kinetics of the H_A^- signal at 675 nm in M214LA reaction centers is similar to M214LG (Figure 3b). This presumably arises because the overall decay of H_A^- is the sum of the rates of charge recombination between P^+ and H_A^- and forward electron transfer from H_A^- to Q_A, and the relative rates of these two processes are different in M214LA and M214LG reaction centers.

Analysis of Kinetics. Fitting of the time-resolved spectra described above to a sum of exponentials shows that the nearly single exponential decay of the H_A^- signal at 675 nm in wild type reaction centers is decidedly more complex in the M214 mutants, with kinetic components of hundreds of picoseconds and several nanoseconds well resolved (Figure 3b). The time-resolved spectral surfaces were fitted simultaneously in the Q_X and Q_Y spectral regions using a sequential, irreversible kinetic model. The amplitude spectra obtained in this way are referred to as evolution-associated difference spectra (EADS).[50] These spectra are not meant to represent the actual states present at any given time (it may well be that the reactions involved are neither sequential nor irreversible), but they provide a simple means of visualizing the progression of spectral changes as a function of time and describing the quantitative results of the fitting. Because the model involves irreversible reactions, the time constants are simply those from the exponential fit itself. For the wild type and M214LM reaction centers, five exponential decay times (and thus five EADS spectra and associated time constants) were required to describe the time-resolved spectra. For the other three mutants, six states were required. The initial electron transfer from P* forming $P^+H_A^-$ has previously been shown to be multiexponential in the wild type reaction centers.[51−53] Consistent with this, the first three EADS had time constants of 2.8−3.5 ps, 0.9 ps, and 10−12 ps in the wild type and all four M214 mutant reaction centers. These three time constants are also consistent with the similarity of the observed P* decay kinetics and the electrochromic shift signals from B_A in Figure 2 panels a and b. The spectrum of each of the three initial EADS for the wild type reaction center are similar to previous reports[51,53] and are shown in Figure S-2 of the Supporting Information.

In contrast to the picosecond EADS, the EADS on the hundreds of picosecond to nanosecond time scales are distinct between the wild type and the M214LC, M214LA and M214LG mutants. As in other respects, M214LM is very similar to wild type on all time scales (Figure S-1, Supporting Information). For the wild type reaction center, the fourth EADS component has an exponential decay time of 220 ps ($P^+H_A^- \rightarrow P^+Q_A^-$) and the fifth EADS component is non-decaying; i.e., its lifetime is much longer than the 6 ns time window of the measurement. The EADS of these two components are shown in Figure 4e and consist of spectral features well documented for $P^+H_A^-$ and $P^+Q_A^-$, respectively.[54−56] Both the H_A ground-state bleaching at 540 nm and the H_A^- absorbance at 660 nm are present in the 220-ps EADS (Figure 4e, red curve), and then disappear in the non-decaying EADS (Figure 4e, black curve), whereas the P ground-state bleaching bands associated with P^+ at 600 and 865 nm are unchanged between the two EADS.

The lifetime of the EADS component on the hundreds of picosecond time scale progressively increases for the mutants M214LC, M214LA, and M214LG (250 ps, 290 ps, and 330 ps, respectively). Moreover, an additional component on the order of several nanoseconds (an additional EADS) is required, which accounts for the kinetic heterogeneity in the spectral evolution of the absorbance changes. In the mutant M214LC (Figure 4f), at least part of the heterogeneity apparently arises because electron transfer from H_A^- to Q_A occurs with more than one rate. About half of the formation of $P^+Q_A^-$, that is, decay of the H_A^- signals, occurs in the time between the 250 ps EADS and the 6−10 ns EADS, whereas there is essentially no decay of P^+ (the ground state bleaching of P at 865 nm remains constant). However, during the subsequent transition between the 6−10 ns EADS and the non-decaying EADS, there is substantial loss of both the P^+ and H_A^- signals. As the amount of the H_A^- signal recovery on the nanosecond time scale is ~50% relative to its maximum in the 250-ps EADS and the P^+ signal recovers less than 30% over the same period, it is reasonable to suggest that both $H_A^- \rightarrow Q_A$ electron transfer and $P^+H_A^-$ recombination occur during this time period. Apparently, recombination of $P^+H_A^-$ competes effectively with forward electron transfer in the population of $P^+H_A^-$ in which transfer to Q_A takes place over the 6−10 ns time period. This could happen only if the forward electron transfer rate were substantially slower than 200 ps for this population of reaction centers. In fact, the rate constant for the slow component of the electron transfer to Q_A in this case must be many nanoseconds, because the 6−10 ns kinetic transition represents roughly the sum of the rates of forward transfer and recombination. As the spectral characteristics of the 6−10 ns EADS reflect a combination of $P^+H_A^-$ and $P^+Q_A^-$, the kinetic complexity observed is presumably due to either static heterogeneity of the reaction center with respect to $P^+H_A^-$ (i.e., there are multiple, functionally different populations of reaction centers with

dx.doi.org/10.1021/jp400132k | J. Phys. Chem. B XXXX, XXX, XXX−XXX

Table 1. Populations of $P^+H_A^-$, $P^+B_A^-$, and $P^+Q_A^-$ in each EADS Shown in Figure 4 Panels e–h. See Text for Details

	WT		LC		LA		LG		
	$[P^+H_A^-]$	$[P^+Q_A^-]$	$[P^+H_A^-]$	$[P^+Q_A^-]$	$[P^+H_A^-]$	$[P^+Q_A^-]$	$[P^+B_A^-]$	$[P^+H_A^-]$	$[P^+Q_A^-]$
hundred picosecond	1.00	0.00	1.00	0.00	1.00	0.00	0.15	0.85	
nanosecond	NA[a]	NA[a]	0.48	0.52	0.79	0.19	0.05	0.68	0.10
non-decaying	0.00	1.00	0.14	0.62	0.36	0.24		0.40	0.10

[a]NA = not applicable.

different $H_A^- \rightarrow Q_A$ electron transfer rates), or the heterogeneity is due to dynamic relaxation of $P^+H_A^-$ (or some combination). Both possibilities will be modeled in the Discussion section. In the M214LA mutant reaction center, the situation is similar (Figure 4g), except that the faster component of the forward transfer from H_A^- to Q_A is slightly slower than that in M214LC, and thus the overall yield of $P^+Q_A^-$ formation is lower. It is worth mentioning that there is still some $P^+H_A^-$ remaining in the non-decaying EADS in both the M214LC and M214LA mutants, that is, some of the $P^+H_A^-$ do not undergo the $H_A^- \rightarrow Q_A$ electron transfer, a topic that will be discussed in more detail below. In the M214LG reaction center, very little spectral evidence of $P^+Q_A^-$ formation was found on any time scale (Figure 4h). Again, three EADS with time constants of several hundred picoseconds, 4–6 ns, and a non-decaying component are adequate to fit the two spectral regions globally. In this case, the lifetime of the faster EADS is about 330 ps in the Q_X region, while it is about 430 ps in the Q_Y region (Figure 4h, red curve). This suggests that the kinetic complexity is greater than the number of EADS used can uniquely describe (this issue is addressed elsewhere, but may involve electrochromic shifting of the reaction center ground state absorbance bands). In contrast to the situation described above for the M214LC and M214LA mutants, in which there was no loss of P^+ on this time scale, there is a significant decrease in bleaching at 865 nm in the M214LG mutant between the several hundred ps EADS and the 4–6 ns EADS. This indicates that charge recombination between H_A^- and P^+ occurs even on a subnanosecond time scale.

DISCUSSION

The most striking feature of this series of M214 mutants is that single amino acid changes in the immediate vicinity of H_A have large effects on secondary electron transfer from H_A^- to Q_A but not on primary electron transfer from P* to H_A. This implies that parameters other than simply the static energetics of $P^+H_A^-$ in the mutants have been changed. Changes in both the spectral and kinetic properties of these mutants are strongly correlated with the volume of the amino acid that replaced the leucine residue at the M214 position (the smaller the volume the more significant the difference from wild type), suggesting that a change in protein flexibility may be involved.

Recently the structure of the M214LG mutant has been solved to a resolution of 2.2 Å. Although the positions of the H_A and Q_A cofactors are largely preserved, two conformations of the phytyl tail of B_A were revealed.[57] Molecular dynamics simulations suggest that the conversion between the two conformations of the phytyl tail involve a large scale protein rearrangement (LeBard et al., private communication). This is again consistent with the notion that the mutants are more flexible than the wild type. This added flexibility could manifest itself in the complex dynamics observed for the $H_A^- \rightarrow Q_A$ reaction in two general ways: either there is more than one reaction center conformation present and that conformational heterogeneity is static on the time scale of the $H_A^- \rightarrow Q_A$ electron transfer, or the flexibility manifests as a dynamic relaxation process that affects the electron transfer reaction (or both). These possibilities are explored below.

$P^+H_A^-$ and $P^+Q_A^-$ Populations in Different Intermediate States. To quantitatively compare the effects of the different mutations at M214, each of the EADS spectra derived from fitting were linearly deconvoluted into contributions from $P^+H_A^-$ and $P^+Q_A^-$. For this analysis, the Q_X spectral region of the EADS was used because there are major features associated with both P^+ and H_A^- in this region. In wild type reaction centers, the spectra of $P^+H_A^-$ and $P^+Q_A^-$ are easy to determine given their very different lifetimes. Electron transfer from H_A^- to Q_A occurs with a relatively homogeneous time constant of 220 ps and a yield of essentially 100%. $P^+Q_A^-$ lives for 100 ms[7] (compare this to the 6 ns time scale of current measurement), and therefore the non-decaying spectra of the EADS represents essentially pure $P^+Q_A^-$. The 220-ps EADS is taken to represent pure $P^+H_A^-$, as it is well separated kinetically from both P* and $P^+Q_A^-$ on this time scale. In the mutants, however, $P^+H_A^-$ and $P^+Q_A^-$ are generally not well separated kinetically and the EADS are mixtures of these spectra.

Each of the three EADS of the mutants that showed large effects (M214LC, M214LA, and M214LG) was fitted to a linear combination of the wild type $P^+H_A^-$ and $P^+Q_A^-$ spectra using the expression EADS = $h[P^+H_A^-] + q[P^+Q_A^-]$, where h and q are coefficients that specify the amount of $P^+H_A^-$ and $P^+Q_A^-$ in the EADS, relative to the initial amount of P* formed ($h + q$ will not necessarily be 1.0 if there is ground state recovery during charge separation). The fitting procedures and estimated errors are described in detail in the Supporting Information, and the results are summarized in Table 1.

For M214LC and M214LA, a nearly pure (within 5%) $P^+H_A^-$ population is found in the EADS that has a lifetime of hundreds of picoseconds (Supporting Information, Figure S-3, LC and LA). The M214LG EADS on this time scale, in contrast, contains only ~85% of the $P^+H_A^-$ population. However, the remaining 15% of the charge separated state is not $P^+Q_A^-$. The M214LG EADS shows a larger absorbance decrease at 600 nm and smaller decrease at 540 nm than is observed in wild type reaction centers, indicative of a population of $P^+B_A^-$ (Supporting Information, Figure S-3, LG).

The nanosecond EADS in all three mutants appears to represent a mixture of $P^+H_A^-$ and $P^+Q_A^-$ (Table 1). The populations of these two states are 48% and 52%, respectively, of the total initial population for the M214LC reaction centers, and 79% and 19%, respectively, for the M214LA reaction centers. There do not appear to be any additional spectral states present, nor is there any substantial ground state recovery on subnanosecond time scales in these two mutants, in agreement with the fact that the P bleaching at 865 nm is essentially identical between the hundreds of picosecond and nanosecond EADS (Figure 4f and g). In contrast, the M214LG mutant

dx.doi.org/10.1021/jp400132k | J. Phys. Chem. B XXXX, XXX, XXX–XXX

reaction centers give rise to an EADS on the nanosecond time scale that is 70% $P^+H_A^-$ and 10% $P^+Q_A^-$. The remaining ~20% of the M214LG reaction centers appears to have recombined to the ground state on the subnanosecond time scale, something not observed in any of the other samples. In reasonable agreement with this, there is a 12% amplitude loss of the P^+ bleaching at 865 nm between the hundreds of picoseond EADS and the 4−6 ns EADS.

The EADS that is non-decaying on the time scale of the measurement represents a mixture of $P^+Q_A^-$ and $P^+H_A^-$ in all three mutants. Approximately 14%, 36%, and 40% of the $P^+H_A^-$ population remains in the non-decaying EADS in the M214LC, M214LA, and M214LG reaction centers, respectively (Table 1). This $P^+H_A^-$ component of the spectrum is presumably decaying on the many nanosecond time scale, but because the total time scale of the measurement is only 6 ns, the expected 10−20 ns lifetime of $P^+H_A^-$ in the absence of forward electron transfer (or with very slow electron transfer) becomes mixed with the much longer lived (millisecond) $P^+Q_A^-$ component. However, there is some forward electron transfer taking place in both M214LC and M214LA reaction centers; comparison of the nanosecond and non-decaying EADS spectra (Figure 4f−h) indicates that there is a 10% and 5% increase in $P^+Q_A^-$ population in going from the former to the latter EADS in M214LC and M214LA, respectively (Table 1). In contrast, M214LG mutant reaction centers do not appear to form additional $P^+Q_A^-$ during this time.

A substantial amount of charge recombination takes place on the nanosecond time scale in all three mutants; that is, the total amount of bleaching at 865 nm due to P^+ decreases as some of the reaction centers return to the ground state. This is expected when $P^+H_A^-$ persists for nanoseconds. Note that there is rough agreement between the total amount of P^+ estimated during the spectral fitting in the Q_X region of the spectrum for each of the mutants and the amount predicted from the extent of bleaching at 865 nm (compare the P ground state band recovery in Figure 4f−h and the total P^+ population for the non-decaying component in Table 1).

Reaction Scheme. As described above, three of the four RC mutants studied in this work (M214LC, M214LA, and M214LG) show kinetic complexity on the hundreds of picoseconds to nanoseconds time scale that is not observed in wild type or M214LM. The heterogeneity that gives rise to such complexity could either be static (multiple reaction center conformations), dynamic (time-dependent protein relaxation), or some combination of the two. Reaction schemes representing the two extreme forms of these models were constructed based on the results from the EADS analysis of Table 1 and are shown in Figure 4. Because the major kinetic differences between the mutants are observed during the $H_A^- \rightarrow Q_A$ electron transfer, the reaction schemes discussed below start from the state(s) represented in the EADS with a time constant of hundreds of picoseconds. This spectrum is dominated in all cases by $P^+H_A^-$ formed during initial electron transfer.

One could explain the kinetically complex spectral evolution on the hundred picosecond time scale in terms of static heterogeneity by supposing that several functionally distinct populations of $P^+H_A^-$ are formed in the mutants during initial electron transfer and that these different populations then behave distinctly during the subsequent electron transfer reaction (Figure 4a−d). In this case, the estimated subpopulations of $P^+H_A^-$, $P^+Q_A^-$ and the ground state in Table 1 result from kinetically distinct reactions in different reaction center subpopulations. In M214LC and M214LA, this model would suggest that one $P^+H_A^-$ population behaves more or less like wild type and undergoes forward electron transfer to Q_A on the few hundred picosecond time scale. A second $P^+H_A^-$ population has an observed lifetime in the 6−10 ns time range, and decays by two routes: part recombines to the ground state with a roughly 10 ns lifetime (in rough agreement with the lifetime of $P^+H_A^-$ in RCs with Q_A removed) and part undergoes electron transfer to Q_A on an even longer time scale. A third $P^+H_A^-$ population in this model does not undergo the $H_A^- \rightarrow Q_A$ electron transfer and presumably decays to the ground state on the 10−20 ns time scale. The microscopic time constants shown in Figure 4a−d were calculated according to the equation: $\tau_{ET} = \tau_{obs}/\phi_{ET}$, where ϕ_{ET} is the population of $P^+H_A^-$ obtained from the fitting of the EADS (described above), and τ_{obs} is the observed time constant associated with the EADS obtained in the fit.

The application of the static model to M214LG requires a somewhat different scheme. In this case, even the shortest lifetime form of $P^+H_A^-$ decays in part via recombination to the ground state, and the longer-lived $P^+H_A^-$ populations decay entirely via recombination (although with two different time constants). While this is a formal possibility, it requires two rather *ad hoc* assumptions. First, the characteristics of one population of $P^+H_A^-$ are such that it recombines rapidly enough to compete with electron transfer to Q_A on the few hundred picosecond time scale and yet does not appreciably change the rate of forward electron transfer from P* to $P^+H_A^-$. It is difficult to understand, if this really represents a single, static state, how one reaction could be affected so profoundly without significantly affecting the other. Second, this possibility requires the assumption that there are two additional forms of $P^+H_A^-$ that recombine with different rates. This is plausible, the two forms could have different reaction free energies, but again, both of these forms of $P^+H_A^-$ in this model are directly created from P* with a rate that is not substantially different from wild type. Similar arguments also apply to the explanation of the M214LC and M214LA data using the static heterogeneity model, though to a lesser extent.

It is also possible to model the kinetics purely in terms of dynamic heterogeneity (Figure 4i−l). In this model, the complex reaction kinetics described above can be explained by introducing a relaxation in the energy of $P^+H_A^-$ on the hundreds of picosecond to several nanosecond time scale. A key aspect of this scheme is that the form of $P^+H_A^-$ generated initially from P* is different from the form that is formed by further relaxation, at least in the mutants, explaining how the initial electron transfer could be very similar to wild type but recombination and forward electron transfer to Q_A could be substantially different from wild type. The initial form of $P^+H_A^-$, $(P^+H_A^-)_i$, can either undergo electron transfer forming $P^+Q_A^-$, recombine regenerating the ground state, or relax to form intermediate states $(P^+H_A^-)_m$ and $(P^+H_A^-)_f$. In quinone-containing wild type reaction centers, the only pathway of significance is forward electron transfer, but in the mutants, relaxation takes place before transfer to Q_A is complete, and the kinetic complexity can be explained by supposing that relaxation of $P^+H_A^-$ results in a decrease in the forward electron transfer rate constant. The time constant expected for recombination, based on measurements in wild type reaction centers that lack Q_A, is 10−20 ns.[24,25] Thus in the mutants, one would expect that if the relaxation of $P^+H_A^-$ led to the slowed

dx.doi.org/10.1021/jp400132k | J. Phys. Chem. B XXXX, XXX, XXX−XXX

or stopped forward electron transfer, substantial ground state recovery would take place, as observed in the mutants on the nanosecond time scale (Figure 4f–h). Using this model, yields and rate constants associated with each reaction pathway can be estimated from the observed time constants and the spectral deconvolution of the EADS described above (Figure 4i–l, Tables 2 and 3, details given in Supporting Information). In the case of the M214LA and the M214LC substitutions, forward electron transfer dominates on the several hundred picosecond time scale (there is no ground state recovery of the 865 nm P band due to recombination). However, on the 6–10 ns time scale, substantial charge recombination occurs. In the M214LG substituted mutant, significant ground state recovery (recovery of the 865 nm bleaching of P) takes place even on the few hundred picosecond time scale. This can only happen if the recombination rate is substantially increased in this mutant in the form of $P^+H_A^-$ that is present on that time scale. Table 2 provides a summary of the overall yields of $P^+Q_A^-$ and the final relaxed form of $P^+H_A^-$.

Table 2. Final Yields (ϕ) along Each Reaction Pathway from $(P^+H_A^-)_i$ Shown in Figure 4 panels i–l

RC sample	WT	LC	LA	LG
ϕ_{ET}%[a]	100	62	24	10
ϕ_{Trap}%[b]	0	14	36	40
$\phi_{Rec\text{-}i}$%[c]	0	0	0	12
$\phi_{Rec\text{-}m}$%[d]	0	25	30	35
ϕ_{Sum}%[e]	**100**	**101**	**90**	**97**

[a]Total yield of $P^+Q_A^-$, i.e. coefficient "q" obtained from fitting the non-decaying EADS using equation EADS = $h[P^+H_A^-]+ q[P^+Q_A^-]$. [b]The population of reaction centers trapped in the $P^+H_A^-$ state calculated from coefficient "h" from fitting the non-decaying EADS. [c]Yield loss due to $P^+H_A^-$ recombination, calculated from the amplitude decrease of the P^+ signal (bleaching of the Q_Y band of P) when evolving from the hundreds of picosecond to nanosecond EADS. [d]Yield loss due to recombination of the relaxing $P^+H_A^-$ state, calculated from the amplitude decrease of the P^+ signal (bleaching of the Q_Y band of P) when evolving from the nanosecond to the non-decaying EADS. [e]The sum of yields from the first four rows.

Table 3. Kinetic Rates (τ_{obs}) from Global Analysis and Electron Transfer Yields (ϕ) and Rates (τ_{ET}) from the Unrelaxed Form of H_A^- in Wild Type and Mutant Reaction Centers. 100% Yield Is Assumed in Wild Type

RC sample	WT	LC	LA	LG
τ_{obs}[a]	220 ps	250 ps	290 ps	330 ps
ϕ_{ETi}[b]	100%	52%	19%	10%
τ_{ET}[c]	0.22 ns	0.48 ns	1.53 ns	3.30 ns

[a]Observed lifetime of the $(P^+H_A^-)_i$ state, obtained from global fitting using a sequential model. [b]Yield of election transfer from $(H_A^-)_i$ to Q_A, obtained from the amplitude of $[P^+Q_A^-]$ in fitting the nanosecond EADS (Table 1). [c]Calculated time constant for $P^+H_A^- \rightarrow P^+Q_A^-$ electron transfer, using equation $\tau_{ET} = \tau_{obs} / \phi_{ETi}$, which only calculates $P^+Q_A^-$ formation from the $(P^+H_A^-)_i$ state.

Electron Transfer Coupled to Protein Motion on Different Time scales. The purely static and purely dynamic models of electron transfer in this system are, of course, extremes. Proteins are capable of motion on many time scales and have many degrees of freedom. Thus, what is static for electron transfer on the picosecond time scale may be dynamic on the several hundred picosecond or nanosecond time scale. Indeed the crystal structure of the M214LG mutant shows two distinct conformations,[57] and molecular dynamics simulations suggest that these conformations have a large energy barrier between them, making rapid transition between them impossible (LeBard et al., private communication). However, as discussed above, it is not possible to describe the kinetics of electron transfer in this mutant with just two static states, and even models with additional states leave one wondering how, in a static system that so strongly affects the $H_A^- \rightarrow Q_A$ reaction, the initial, picosecond electron transfer reaction is so constant. A key point here is that evolution has both static structure and dynamics on many time scales at its disposal to optimize reactions. Particularly in cases such as this, where one reaction intermediate ($P^+H_A^-$) is involved in at least three reactions on three different time scales (initial electron transfer from P*, forward electron transfer to Q_A, and recombination) that need to be simultaneously adjusted for optimum yield, one might well expect that this optimization would take advantage of structural changes that affect the dynamics on one time scale and not another. It may be, for example, that there is a dynamic evolution of the reaction center on the tens of picosecond time scale resulting in multiple states that are more or less static on the time scale of electron transfer to the quinone. As a result, electron transfer remains largely unperturbed on the picosecond time scale while being strongly altered at longer times in a manner that seriously impairs reaction center function. Similarly, certain mutations at M210 have also been found to affect electron transfer on different time scales in very different ways, presumably for similar reasons.[36] Apparently, wild type reaction center structure has been optimized over a wide range of time scales to avoid these kinds of problems.

Mutational Effects are Correlated with Side Chain Volume. In essentially all aspects of functional change, the effects of the mutants studied can be ordered as follows: (WT or M214LM); M214LC; M214LA; M214LG. The decreasing yield of $P^+Q_A^-$ and the increasingly heterogeneous kinetics appear to correlate with the volume of the amino acid side chain. This makes sense in the context of the thesis presented above: altering the amino acid at M214 can change the dynamic environment for electron transfer on some scales and not on others. Presumably, as smaller and smaller side chains are used, the reaction center becomes increasingly flexible in that area. This may have little effect on initial electron transfer if the ground state positions and effective redox potentials of the cofactors involved remain unchanged. However, upon introduction of a charge pair, a substantial opportunity for relaxation is presented, and added flexibility may well change the rate and extent of that relaxation and thus the time course of charge-separated state energetics.

CONCLUDING REMARKS

In exactly what way the functionally important heterogeneity (dynamic and/or static) is altered upon decreasing the volume of the M214 amino acid side chain is not entirely clear. For example, there is no evidence for ordered electron density (e.g., water) in the cavity observed in the M214LG crystal structure that might imply a specific kind of dielectric relaxation. In any case, it is becoming increasingly evident that reaction center protein dynamics has been preprogrammed to optimize the yields of specific reaction pathways on specific time scales, and that this dynamics and associated heterogeneity are very sensitive to even relatively small structural perturbation. To

dx.doi.org/10.1021/jp400132k | J. Phys. Chem. B XXXX, XXX, XXX–XXX

obtain a deeper understanding of the role of heterogeneity and dynamics in reaction center function, it will be necessary to study the results from these kinds of specific mutants in terms of dynamic structural models.

■ ASSOCIATED CONTENT

Supporting Information

Comparison of transient absorption spectra of wild type and M214LM mutant reaction centers at 25 ps and 6 ns delay after laser excitation at 865 nm in the Q_X and Q_Y transition regions; the three initial EADS (of five total) in the Q_X and Q_Y transition regions for wild type reaction centers, obtained from a global fitting using a sequential kinetic model A→ B→ C→D→E, and subsequent decomposition of the $P^+H_A^-$ and $P^+Q_A^-$ populations in the associated EADS. This material is available free of charge via the Internet at http://pubs.acs.org.

■ AUTHOR INFORMATION

Corresponding Author

* (J.P.) E-mail: JiePan@umich.edu. Tel: 734-936-6863. Fax: 734-764-5153. (N.W.W.) E-mail: Nwoodbury@asu.edu. Tel.: 480-965-3294. Fax: 480-727-0396.

Present Address

#(J.P.) Department of Physics, University of Michigan, Ann Arbor, MI 48109.

Notes

The authors declare no competing financial interest.

■ ACKNOWLEDGMENTS

We thank Drs. D. Matyushov, D. LeBard, and D. Martin for intriguing discussions. This work was funded by NSF Grant MCB-0642260 at ASU. J.T.B. thanks NSERC Canada for funding through the Discovery Grants system, and R. Saer was supported by a postgraduate scholarship from NSERC.

■ ABBREVIATIONS

BChl, bacteriochlorophyll; BPhe, bacteriopheophytin; P, primary electron donor; B_A and B_B, monomer BChls; H_A and H_B, bacteriopheophytins; Q_A and Q_B, quinone; EADS, evolution-associated difference spectra

■ REFERENCES

(1) Kirmaier, C.; Holten, D. Primary Photochemistry of Reaction Centers from the Photosynthetic Purple Bacteria. *Photosynth. Res.* **1987**, *13*, 225−260.

(2) Parson, W. W.; Warshel, A. Mechanism of Charge Separation in Purple Bacterial Reaction Centers. In *The Purple Phototrophic Bacteria*; Hunter, C. N., Daldal, F., Thurnauer, M. C., Beatty, J. T., Eds.; Springer: Dordrecht, The Netherlands, 2009; Vol. *28*, pp 355−377.

(3) Woodbury, N. W.; Allen, J. P. The Pathway, Kinetics and Thermodynamics of Electron Transfer in Wild Type and Mutant Reaction Centers of Purple Nonsulfur Bacteria. In *Anoxygenic Photosynthetic Bacteria*; Blankenship, R. E., Madigan, M. T., Bauer, C. E., Eds.; Kluwer Academic Publishers: Dordrecht, The Netherlands, 1995; Vol. *2*, pp 527−557.

(4) Parson, W. W.; Warshel, A. Dependence of Photosynthetic Electron-transfer Kinetics on Temperature and Energy in a Density-matrix Model. *J. Phys. Chem. B.* **2004**, *108*, 10474−10483.

(5) Warshel, A.; Chu, Z. T.; Parson, W. W. Dispersed Polaron Simulations of Electron-Transfer in Photosynthetic Reaction Centers. *Science* **1989**, *246*, 112−116.

(6) Gehlen, J. N.; Marchi, M.; Chandler, D. Dynamics Affecting the Primary Charge-Transfer in Photosynthesis. *Science* **1994**, *263*, 499−502.

(7) McMahon, B. H.; Muller, J. D.; Wraight, C. A.; Nienhaus, G. U. Electron Transfer and Protein Dynamics in the Photosynthetic Reaction Center. *Biophys. J.* **1998**, *74*, 2567−2587.

(8) Wang, H. Y.; Lin, S.; Allen, J. P.; Williams, J. C.; Blankert, S.; Laser, C.; Woodbury, N. W. Protein Dynamics Control the Kinetics of Initial Electron Transfer in Photosynthesis. *Science* **2007**, *316*, 747−750.

(9) Kotelnikov, A. I.; Medvedev, E. S.; Stuchebrukhov, A. A.; Goryachev, N. S.; Psikha, B. L.; Ortega, J. M. Protein Dynamics Control of Electron Transfer in Reaction Centers from *Rps. viridis*. *Biochim. Biophys. Acta* **2006**, 281−282.

(10) Jones, M. R. The Petite Purple Photosynthetic Powerpack. *Biochem. Soc. Trans.* **2009**, *37*, 400−407.

(11) Wraight, C. A.; Gunner, M. R. The Acceptor Quinones of Purple Photosynthetic Bacteria−Structure and Spectroscopy. In *The Purple Phototrophic Bacteria*; Hunter, C. N., Daldal, F., Thurnauer, M. C., Beatty, J. T., Eds.; Springer: Dordrecht, The Netherlands, 2009; Vol. *28*, pp 379−405.

(12) Allen, J. P.; Feher, G.; Yeates, T. O.; Komiya, H.; Rees, D. C. Structure of the reaction center from *Rhodobacter sphaeroides* R-26: the cofactors. *Proc. Natl. Acad. Sci. U.S.A.* **1987**, *84*, 5730−5734.

(13) Koepke, J.; Krammer, E. M.; Klingen, A. R.; Sebban, P.; Ullmann, G. M.; Fritzsch, G. pH Modulates the Quinone Position in the Photosynthetic Reaction Center from *Rhodobacter sphaeroides* in the Neutral and Charge Separated States. *J. Mol. Biol.* **2007**, *371*, 396−409.

(14) Zinth, W.; Wachtveitl, J. The First Picoseconds in Bacterial Photosynthesis - Ultrafast Electron Transfer for the Efficient Conversion of Light Energy. *ChemPhysChem.* **2005**, *6*, 871−880.

(15) Holzapfel, W.; Finkele, U.; Kaiser, W.; Oesterhelt, D.; Scheer, H.; Stilz, H. U.; Zinth, W. Initial Electron-Transfer in the Reaction Center from *Rhodobacter sphaeroides*. *Proc. Natl. Acad. Sci. U.S.A.* **1990**, *87*, 5168−5172.

(16) Rockley, M. G.; Windsor, M. W.; Cogdell, R. J.; Parson, W. W. Picosecond Detection of an Intermediate in Photochemical Reaction of Bacterial Photosynthesis. *Proc. Natl. Acad. Sci. U.S.A.* **1975**, *72*, 2251−2255.

(17) Kaufmann, K. J.; Dutton, P. L.; Netzel, T. L.; Leigh, J. S.; Rentzepis, P. M. Picosecond Kinetics of Events Leading to Reaction Center Bacteriochlorophyll Oxidation. *Science* **1975**, *188*, 1301−1304.

(18) Parson, W. W.; Clayton, R. K.; Cogdell, R. J. Excited States of Photosynthetic Reaction Centers at Low Redox Potentials. *Biochim. Biophys. Acta* **1975**, *387*, 265−278.

(19) Shuvalov, V. A.; Parson, W. W. Energies and Kinetics of Radical Pairs Involving Bacteriochlorophyll and Bacteriopheophytin in Bacterial Reaction Centers. *Proc. Natl. Acad. Sci. U.S.A.* **1981**, *78*, 957−961.

(20) Schenck, C. C.; Blankenship, R. E.; Parson, W. W. Radical-Pair Decay Kinetics, Triplet Yields and Delayed Fluorescence from Bacterial Reaction Centers. *Biochim. Biophys. Acta* **1982**, *680*, 44−59.

(21) Ogrodnik, A.; Kruger, H. W.; Orthuber, H.; Haberkorn, R.; Michel-Beyerle, M. E.; Scheer, H. Recombination Dynamics in Bacterial Photosynthetic Reaction Centers. *Biophys. J.* **1982**, *39*, 91−99.

(22) Woodbury, N. W. T.; Parson, W. W. Nanosecond Fluorescence from Isolated Photosynthetic Reaction Centers of *Rhodopseudomonas sphaeroides*. *Biochim. Biophys. Acta* **1984**, *767*, 345−361.

(23) Chidsey, C. E. D.; Kirmaier, C.; Holten, D.; Boxer, S. G. Magnetic Field Dependence of Radical-Pair Decay Kinetics and Molecular Triplet Quantum Yield in Quinone-Depleted Reaction Centers. *Biochim. Biophys. Acta* **1984**, *776*, 424−437.

(24) Tang, C. K.; Williams, J. A. C.; Taguchi, A. K. W.; Allen, J. P.; Woodbury, N. W. $P^+H_A^-$ Charge Recombination Reaction Rate Constant in *Rhodobacter sphaeroides* Reaction Centers is Independent of the P/P^+ Midpoint Potential. *Biochemistry* **1999**, *38*, 8794−8799.

(25) Ogrodnik, A.; Keupp, W.; Volk, M.; Aumeier, G.; Michel-Beyerle, M. E. Inhomogeneity of Radical Pair Energies in Photosynthetic Reaction Centers Revealed by Differences in Recombination

Dynamics of $P^+H_A^-$ When Detected in Delayed Emission and in Absorption. *J. Phys. Chem.* **1994**, *98*, 3432−3439.
(26) Woodbury, N. W.; Parson, W. W.; Gunner, M. R.; Prince, R. C.; Dutton, P. L. Radical-Pair Energetics and Decay Mechanisms in Reaction Centers Containing Anthraquinones, Naphthoquinones or Benzoquinones in Place of Ubiquinone. *Biochim. Biophys. Acta* **1986**, *851*, 6−22.
(27) Peloquin, J. M.; Williams, J. C.; Lin, X.; Alden, R. G.; Taguchi, A. K. W.; Allen, J. P.; Woodbury, N. W. Time-dependent Thermodynamics During Early Electron Transfer in Reaction Centers from *Rhodobacter sphaeroides*. *Biochemistry.* **1994**, *33*, 8089−8100.
(28) Gibasiewicz, K.; Pajzderska, M. Primary Radical Pair P^+H^- Lifetime in *Rhodobacter sphaeroides* with Blocked Electron Transfer to Q_A. Effect of *o*-Phenanthroline. *J. Phys. Chem. B.* **2008**, *112*, 1858−1865.
(29) Pawlowicz, N. P.; Van Grondelle, R.; van Stokkum, I. H. M.; Breton, J.; Jones, M. R.; Groot, M. L. Identification of the First Steps in Charge Separation in Bacterial Photosynthetic Reaction Centers of *Rhodobacter sphaeroides* by Ultrafast mid-Infrared Spectroscopy: Electron Transfer and Protein Dynamics. *Biophys. J.* **2008**, *95*, 1268−1284.
(30) Haffa, A. L. M.; Lin, S.; Katilius, E.; Williams, J. C.; Taguchi, A. K. W.; Allen, J. P.; Woodbury, N. W. The Dependence of the Initial Electron-Transfer Rate on Driving Force in *Rhodobacter sphaeroides* Reaction Centers. *J. Phys. Chem. B.* **2002**, *106*, 7376−7384.
(31) Gunner, M. R.; Dutton, P. L. Temperature and $-\Delta G°$ Dependence of the Electron Transfer from BPh^- to Q_A in Reaction Center Protein from *Rhodobacter sphaeroides* with Different Quinones as Q_A. *J. Am. Chem. Soc.* **1989**, *111*, 3400−3412.
(32) Kirmaier, C.; Gaul, D.; Debey, R.; Holten, D.; Schenck, C. C. Charge Separation in a Reaction Center Incorporating Bacteriochlorophyll for Photoactive Bacteriopheophytin. *Science* **1991**, *251*, 922−927.
(33) Laporte, L.; Kirmaier, C.; Schenck, C. C.; Holten, D. Free-Energy Dependence of the Rate of Electron-Transfer to the Primary Quinone in Beta-Type Reaction Centers. *Chem. Phys.* **1995**, *197*, 225−237.
(34) Curutchet, C.; Kongsted, J.; Muñoz-Losa, A.; Hossein-Nejad, H.; Scholes, G. D.; Mennucci, B. Photosynthetic Light-Harvesting Is Tuned by the Heterogeneous Polarizable Environment of the Protein. *J. Am. Chem. Soc.* **2011**, *133*, 3078−3084.
(35) Gibasiewicz, K.; Pajzderska, M.; Ziolek, M.; Karolczak, J.; Dobek, A. Internal Electrostatic Control of the Primary Charge Separation and Recombination in Reaction Centers from *Rhodobacter sphaeroides* Revealed by Femtosecond Transient Absorption. *J. Phys. Chem. B.* **2009**, *113*, 11023−11031.
(36) Guo, Z.; Woodbury, N. W.; Pan, J.; Lin, S. Protein Dielectric Environment Modulates the Electron-Transfer Pathway in Photosynthetic Reaction Centers. *Biophys. J.* **2012**, *103*, 1979−1988.
(37) Deshmukh, S. S.; Williams, J. C.; Allen, J. P.; Kalman, L. Light-Induced Conformational Changes in Photosynthetic Reaction Centers: Dielectric Relaxation in the Vicinity of the Dimer. *Biochemistry.* **2011**, *50*, 340−348.
(38) Brecht, M.; Radics, V.; Nieder, J. B.; Bittl, R. Protein Dynamics-Induced Variation of Excitation Energy Transfer Pathways. *Proc. Natl. Acad. Sci. U.S.A.* **2009**, *106*, 11857−11861.
(39) Gibasiewicz, K.; Pajzderska, M.; Potter, J. A.; Fyfe, P. K.; Dobek, A.; Brettel, K.; Jones, M. R. Mechanism of Recombination of the $P^+H_A^-$ Radical Pair in Mutant *Rhodobacter sphaeroides* Reaction Centers with Modified Free Energy Gaps Between $P^+B_A^-$ and $P^+H_A^-$. *J. Phys. Chem. B.* **2011**, *115*, 13037−13050.
(40) Friesen, A. D.; Matyushov, D. V. Local Polarity Excess at the Interface of Water with a Nonpolar Solute. *Chem. Phys. Lett.* **2011**, *511*, 256−261.
(41) LeBard, D. N.; Matyushov, D. V. Energetics of Bacterial Photosynthesis. *J. Phys. Chem. B.* **2009**, *113*, 12424−12437.
(42) LeBard, D. N.; Kapko, V.; Matyushov, D. V. Energetics and Kinetics of Primary Charge Separation in Bacterial Photosynthesis. *J. Phys. Chem. B.* **2008**, *112*, 10322−10342.
(43) LeBard, D. N.; Matyushov, D. V. Protein-water Electrostatics and Principles of Bioenergetics. *Phys. Chem. Chem. Phys.* **2010**, *12*, 15335−15348.
(44) Jaschke, P. R.; Saer, R. G.; Noll, S.; Beatty, J. T. Modification of the Genome of *Rhodobacter Sphaeroides* and Construction of Synthetic Operons. *Methods Enzymol.* **2011**, *497*, 519−538.
(45) Tehrani, A.; Beatty, J. T. Effects of Precise Deletions in *Rhodobacter sphaeroides* Reaction Center Genes on Steady-state Levels of Reaction Center Proteins: A Revised Model for Reaction Center Assembly. *Photosynth. Res* **2004**, *79*, 101−108.
(46) Sambrook, J.; Fritsch, E. F.; Maniatis, T. *Molecular cloning: a laboratory manual*; Cold Spring Harbor Laboratory Press: Cold Spring Harbor, N.Y., 1987; Vol. 2nd ed.
(47) Goldsmith, J. O.; Boxer, S. G. Rapid isolation of bacterial photosynthetic reaction centers with an engineered poly-histidine tag. *Biochim. Biophys. Acta* **1996**, *1276*, 171−175.
(48) Pan, J.; Lin, S.; Allen, J. P.; Williams, J. C.; Frank, H. A.; Woodbury, N. W. Carotenoid Excited-State Properties in Photosynthetic Purple Bacterial Reaction Centers: Effects of the Protein Environment. *J. Phys. Chem. B* **2011**, *115*, 7058−7068.
(49) Jailaubekov, A. E.; Song, S. H.; Vengris, M.; Cogdell, R. J.; Larsen, D. S. Using Narrowband Excitation to Confirm that the S* State in Carotenoids is not a Vibrationally-Excited Ground State Species. *Chem. Phys. Lett.* **2010**, *487*, 101−107.
(50) van Stokkum, I. H. M.; Larsen, D. S.; van Grondelle, R. Global and Target Analysis of Time-Resolved Spectra. *Biochim. Biophys. Acta* **2004**, *1657*, 82−104.
(51) Holzwarth, A. R.; Muller, M. G. Energetics and Kinetics of Radical Pairs in Reaction Centers from *Rhodobacter sphaeroides*. A Femtosecond Transient Absorption Study. *Biochemistry* **1996**, *35*, 11820−11831.
(52) Huppman, P.; Arlt, T.; Penzkofer, H.; Schmidt, S.; Bibikova, M.; Dohse, B.; Oesterhelt, D.; Wachtveit, J.; Zinth, W. Kinetics, Energetics, and Electronic Coupling of the Primary Electron Transfer Reactions in Mutated Reaction Centers of *Blastochloris viridis*. *Biophys. J.* **2002**, *82*, 3186−3197.
(53) van Stokkum, I. H. M.; Beekman, L. M. P.; Jones, M. R.; van Brederode, M. E.; van Grondelle, R. Primary Electron Transfer Kinetics in Membrane-Bound *Rhodobacter sphaeroides* Reaction Centers: A Global and Target Analysis. *Biochemistry.* **1997**, *36*, 11360−11368.
(54) van Brederode, M. E.; van Mourik, F.; van Stokkum, I. H. M.; Jones, M. R.; van Grondelle, R. Multiple Pathways for Ultrafast Transduction of Light Energy in the Photosynthetic Reaction Center of *Rhodobacter sphaeroides*. *Proc. Natl. Acad. Sci. U.S.A.* **1999**, *96*, 2054−2059.
(55) Haffa, A. L. M.; Lin, S.; Williams, J. C.; Taguchi, A. K. W.; Allen, J. P.; Woodbury, N. W. High Yield of Long-Lived B-Side Charge Separation at Room Temperature in Mutant Bacterial Reaction Centers. *J. Phys. Chem. B.* **2003**, *107*, 12503−12510.
(56) Kirmaier, C.; Laible, P. D.; Hanson, D. K.; Holten, D. B-Side Charge Separation in Bacterial Photosynthetic Reaction Centers: Nanosecond Time Scale Electron Transfer from H_B^- to Q_B. *Biochemistry.* **2003**, *42*, 2016−2024.
(57) Saer, R. G.; Hardjasa, A.; Rosell, F. I.; Mauk, A. G.; Murphy, M. E. P.; Beatty, J. T. Role of *Rhodobacter sphaeroides* Photosynthetic Reaction Center Residue M214 in the Composition, Absorbance Properties, and Conformations of H_A and B_A Cofactors. *Biochemistry.* **2013**, *52*, 2206−2217.